n-type diamond growth by phosphorus doping on (0 0 1)-oriented surface

2007 J. Phys. D: Appl. Phys. 40 6189

(http://iopscience.iop.org/0022-3727/40/20/S05)

IOP Publishing Journal of Physics D: Applied Physics
J. Phys. D: Appl. Phys. **40** (2007) 6189–6200 doi:10.1088/0022-3727/40/20/S05

n-type diamond growth by phosphorus doping on (0 0 1)-oriented surface

Hiromitsu Kato[1,2], **Toshiharu Makino**[1,2], **Satoshi Yamasaki**[1,2,3] **and Hideyo Okushi**[1,2]

[1] Nanotechnology Research Institute, AIST (National Institute of Advanced Industrial Science and Technology), Tsukuba Center 2, Tsukuba, Ibaraki, 305-8568, Japan
[2] CREST/JST (Japan Science and Technology Corporation), Chiyoda, Tokyo, 102-0081, Japan
[3] Graduate School of Pure and Applied Science, Tsukuba University, Tennodai, Tsukuba, Ibaraki, 305-8577, Japan

E-mail: hiromitsu.kato@aist.go.jp

Received 12 March 2007, in final form 17 May 2007
Published 5 October 2007
Online at stacks.iop.org/JPhysD/40/6189

Abstract
The properties of phosphorus incorporation for n-type doping of diamond are discussed and summarized. Doping of (0 0 1)-oriented diamond is introduced and compared with results achieved on (1 1 1) diamond. This review describes detailed procedures and conditions of plasma-enhanced chemical vapour deposition (CVD) growth and characteristics of electrical properties of phosphorus-doped diamond. The phosphorus incorporation was characterized by SIMS analysis including mapping. n-type conductivity is evaluated by Hall-effect measurements over a temperature regime of 300–1000 K. The crystal perfection of (0 0 1)-oriented n-type diamond is also evaluated by x-ray diffraction, Raman spectroscopy, reflection high-energy electron diffraction and cathodoluminescence analyses. The results show that phosphorus atoms are incorporated into the diamond network during (0 0 1) CVD diamond growth and that phosphorus acts as a donor as in (1 1 1)-oriented diamond. This result eliminates the restriction on substrate orientation, which had previously created a bottleneck in the development of diamond electronic devices.

1. Introduction

Diamond is not only attractive as jewellery but it also possesses excellent physical and electrical properties such as high breakdown voltage, high thermal conductivity, small dielectric constant, wide band gap and excellent radiation hardness [1]. Moreover, since diamond is a group IV element semiconductor, structural defects originating from the alloying effect as seen in III–V semiconductors can be ruled out. Based on these facts, diamond is expected to be a promising wide-band-gap semiconductor for electronic and optical applications, such as ultraviolet light emitting diodes (UV-LED), cold cathode electron emitters and high-power and high-frequency devices [2–11]. In particular, exciton-related devices [12, 13] and electron emitters with negative electron affinity are considered to be future applications utilizing the unique properties of diamond. To realize these applications in practical use, several fundamental technological issues must be resolved including high-quality diamond growth, p- or n-type doping, contact fabrication and etching technology. In particular, n-type doping is the most difficult task to solve and optimize in diamond synthesis.

Since the 1980s, which witnessed the introduction of chemical vapour deposition (CVD) of diamond using microwave plasmas [14], many studies have been carried out on intrinsic diamond growth and on p- or n-type doping by the CVD technique [15–24]. For p-type diamond, the impurity boron, B, is easily incorporated into both natural and synthetic diamond by CVD without any restriction on crystal orientation. The boron acceptor level was determined to be ∼0.37 eV above the top of the valence band. The quality of boron-doped CVD diamond has now reached a maximum mobility of ∼1800 $cm^2\ V^{-1}\ s^{-1}$ at 290 K as determined by Hall-effect measurements [15], which is close to the maximum value of

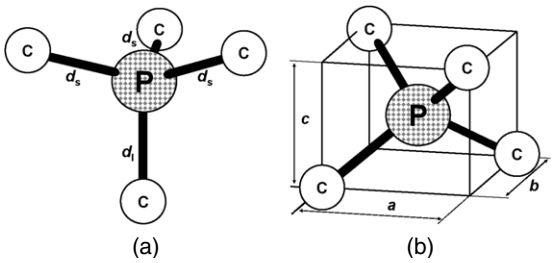

Figure 1. Structure around substitutional phosphorus in diamond [26]. (*a*) Trigonal C_{3v} symmetry, $d_l \sim 1.723$ Å and $d_s \sim 1.693$ Å. (*b*) Tetragonal D_{2d} symmetry, $a = b \sim 1.978$ Å and $c \sim 1.923$ Å. The carbon atoms have a tetrahedral coordination and occupy the lattice sites of the diamond structure.

$\sim$2010 cm^2 V^{-1} s^{-1} obtained for IIb crystals [1]. Superior Schottky junction has also been realized with an ideality factor of $\sim$1.0 [16]. In addition, by means of time-of-flight measurement, a mobility of 3800 cm^2 V^{-1} s^{-1} for holes and 4500 cm^2 V^{-1} s^{-1} for electrons has also been reported for high-quality intrinsic CVD diamond [24].

On the other hand, n-type diamond is not present in nature, and controlled n-type doping had been considered almost impossible until 1997. Among the group V elements, nitrogen was one of the candidates for n-type doping because of its similar covalent bond length (0.74 Å) to that of diamond (0.77 Å), but unfortunately it forms a deep donor level at $\sim$1.7 eV below the bottom of the conduction band, due to its structural distortion from the substitutional position in the diamond lattice [25]. Phosphorus, P, has long been considered as another candidate for n-type doping. In 1997, Koizumi *et al* [18] experimentally demonstrated the growth of n-type diamond on (1 1 1)-oriented diamond substrates by the use of phosphorus and PECVD with a mixture of PH_3, CH_4 and H_2 gas. Following this success, much effort was devoted to growing high-quality P-doped n-type diamond films [19–23] so that currently mobility up to $\sim$660 cm^2 V^{-1} s^{-1} has been achieved [23].

Figure 1 shows the suggested structure around phosphorus in diamond. As phosphorus atoms are incorporated into the substitutional site, structural distortion should occur due to degradation of the site symmetry caused by the difference in covalent bond length between phosphorus (1.10 Å) and carbon (0.77 Å). The electronic structure and stable structure of phosphorus in diamond lattice have been investigated by theoretical calculation [26–30] and experimental study using electron spin resonance (ESR) analyses [31, 32], but are yet to be completely identified. The calculations suggest that the site symmetry of phosphorus is trigonal C_{3V} (figure 1(*a*)) [28], whereas tetragonal D_{2d} (figure 1(*b*)) [31] is suggested by the ESR study of (1 1 1) P-doped diamond. Detailed investigation of this problem is currently ongoing. The phosphorus donor level in diamond was experimentally estimated at $\sim$0.6 eV below the bottom of the conduction band [18–23]. This is much deeper than the calculated values of 0.2–0.4 eV [26–30]. The difference relates to the mode of structural distortion as mentioned above. Moreover, such size mismatch between phosphorus and carbon indicates that some native defects and structural displacement will accompany phosphorus incorporation, which was an aspect preventing diamond n-type control for a long time.

The discovery of phosphorus doping was closely limited to (1 1 1)-oriented diamond lattice structure. For actual technological applications, the growth of n-type diamond films on (0 0 1) substrates is a basic requirement. The (1 1 1) diamond surface is difficult to polish mechanically, whereas it is relatively easy to achieve smooth (0 0 1) surfaces. In the case of non-doped and/or B-doped diamond films, it has been reported that the performance of metal/diamond junction properties as well as electrical and optical properties of films on (0 0 1) surfaces are indeed better than those on (1 1 1) substrates. In addition, (1 1 1)-oriented diamond substrates are difficult to produce, which makes them expensive, and the size is currently limited, which generates significant technological problems with respect to photolithography, etching, metallization and throughput. To bring diamond electronic applications closer to the actual market and to manufacture bipolar devices for a wide range of applications, it is necessary to control n-type doping using phosphorus on (0 0 1)-oriented crystals.

From these viewpoints, there was a strong need for the development of n-type doping on (0 0 1)-oriented diamond. In 2005, we overcame this difficulty by optimizing the conditions for CVD growth, where the parameters differ significantly compared with those for (1 1 1) growth [33, 34]. This is a significant achievement, eliminating the restrictions on crystal orientation of n-type doping. Based on this breakthrough, the fabrication of p–n or p–i–n junctions with good diode characteristics became feasible on (0 0 1)-oriented substrate with all CVD layers and high-efficiency excitonic emission with deep UV light at room temperature could be realized [3, 35]. In this paper, we summarize our research results, including the procedures and conditions of CVD growth, phosphorus incorporation, and characteristic properties and compare it with the features of (1 1 1) P-doped diamond. Recent progress in p–i–n junction UV-LED is also described.

2. Experimental procedures

Homoepitaxial diamond films were grown using a microwave plasma-enhanced CVD reactor consisting of a 6 inch stainless-steel chamber produced by ASTeX. The maximum output microwave power is 1.5 kW and the base pressure of the system can be decreased to 10^{-9} Torr by a turbomolecular pump system with an oil-free scroll pump. Source gases used were CH_4 (purity: 6N) diluted with H_2 (9N) and PH_3 (6N) diluted with H_2 (PH_3/H_2 = 5.0%, 6N). The gas flow rate was controlled independently by mass flow controllers. The substrate temperature was measured by an optical pyrometer from the top window through the plasma and the plasma conditions were monitored by optical emission spectroscopy. The temperature and the plasma emission were confirmed to be stable during CVD growth.

Figure 2 shows a typical emission spectrum during diamond CVD growth in the wavelength region of 200–800 nm. This plasma emission was obtained at an H_2 flow of 397 sccm with CH_4 of 1.6 sccm and PH_3 of 1.6 sccm, microwave power of 750 W and gas pressure of 25 Torr. The spectrum strongly depends on power and pressure. For the described parameters, the following lines and bands were observed: strong hydrogen atomic lines H_α (656.3 nm), H_β

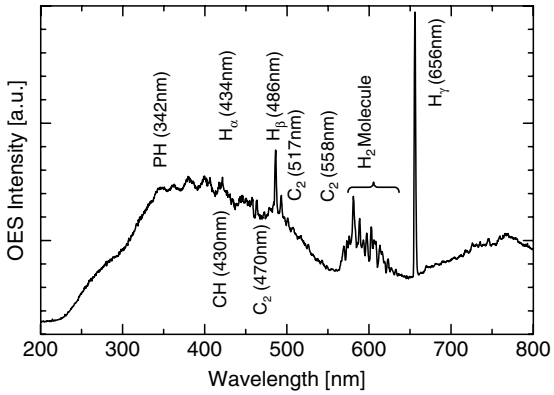

Figure 2. Optical emission spectrum of microwave plasma during CVD growth. Plasma conditions: microwave power, 750 W; pressure, 25 Torr; total gas flow, 400 sccm; $[CH_4]/[H_2]$; 0.4%; $[PH_3]/[CH_4]$; 5.0%.

(486.1 nm) and H_γ (434.0 nm), H_2 molecular lines, CH 430.0 nm system ($A^2\Delta$–$X^2\Pi$) and C_2 swan system ($A^3\Pi_g$–$X'^3\Pi_u$). A phosphorus related line was also observed in 342.0 nm of PH ($A^3\Pi$–$X^3\Sigma$), the intensity of which depended on the $[PH_3]$ gas flow rate. All these peaks are identified by [36].

Before CVD growth, all the substrates were re-polished to reduce the mechanical polishing patterns observed by optical microscopy in the Nomarski mode and then cleaned by the following chemical treatment. Firstly, the substrate is boiled in an acid mixture ($H_2SO_4 : H_2O_2 : H_2O$, 3 : 1 : 1) at 220 °C for 15 min to remove organic and metallic contamination from the surface, followed by HF treatment for 5 min to remove SiO_2 and metallic contamination, and then the substrate is again boiled in SC1 ($NH_4OH : H_2O_2 : H_2O$, 1 : 1 : 5) at 75 °C for 15 min to remove particles and organic contamination. After each chemical treatment, substrates are rinsed with deionized water. The cleaned substrate is then set on a molybdenum holder coated by a diamond layer and placed in the CVD growth system.

For CVD growth, a three-step method was applied [34]. The first step was surface cleaning and stabilization of the CVD environment (plasma, pressure, temperature, etc). The second step was improving the initial surface by means of ultra-low CH_4 admixture to H_2, giving rise to very slow growth [37]. The third step was the CVD diamond film growth. This method is useful for obtaining reproducibility with a smooth surface and growing high-quality films.

Substrates used were commercially available type IIa and Ib diamond crystals with (0 0 1)-oriented surface, which were synthesized by a high-temperature, high-pressure (HTHP) method. The substrate size was 3.0 × 3.0 × 0.5 mm^3 and 2.5 × 2.5 × 0.5 mm^3 for Ib and IIa crystals, respectively. The misorientation angle of all diamond substrates used in this experiment was measured by x-ray diffraction (XRD), Raman spectroscopy and ESR analysis.

The incorporation of phosphorus and other impurities was evaluated using secondary-ion mass spectroscopy (SIMS). As primary ions, Cs^+ accelerated at 14.5 keV was used for P, N, B and Si atoms, and O_2^+ accelerated at 8.0 keV was used for Cu, Fe, Mo and W atoms. The concentrations of P, N and B atoms were quantified using implanted standard samples. The spatial distribution of hydrogen atoms was determined by the SIMS mapping technique. The scanning area was 25 × 25 μm^2 and the spatial resolution was ∼1 μm^2.

The XRD rocking-curve measurements were performed using a Bede D1 diffractometer system with $CuK_{\alpha 1}$ radiation. Two germanium monochromator crystals were used in combination with Ge (0 0 4) diffraction, which provided the primary x-ray beam. During rocking-curve measurements the detector with an open aperture was set to the diamond (0 0 4) Bragg angle. Confocal Raman spectra were applied using the 514 nm line of an Ar laser. Back-scattered light was dispersed in a 1 m double monochromator system and detected by a charge-coupled device (CCD) array. Raman spectra parameters (frequency and bandwidth) were obtained by a least-squares fit of Lorentzian functions to the experimental data. Cathodoluminescence analyses were performed using a scanning electron microscope in combination with an optical system comprising an ellipsoidal mirror, optical fibre and monochromator, equipped with a liquid-nitrogen-cooled CCD array. CL observations were performed at an electron energy of 10 kV, where the penetration length of electrons is about ∼1 μm.

Electrical properties were investigated by Hall-effect measurements in the van der Pauw contact configuration as a function of temperature from room temperature to 1000 K, applying an oscillating magnetic field method using ∼0.6 T field strength. As-grown diamond films were boiled in an acid mixture ($H_2SO_4 : HNO_3$, 3 : 1) at ∼220 °C for 30 min to remove surface hydrogen. Contact electrodes of Ti (30 nm)/Pt (30 nm)/Au (100 nm) were evaporated through a shadow mask with four symmetrically located holes and then annealed at 420 °C for 30 min in Ar atmosphere in order to achieve stable contact between the diamond and Ti.

3. Comparison between organic and hydride phosphorus source gases

The careful selection of a proper source gas is important for doping of semiconductors by the CVD technique, since different gases lead to different growth kinetics and film properties. Detailed properties of organophosphorus, tertiarybutylphosphine (TBP: $P(C_4H_9)H_2$)) and trimethylphosphine (TMP: $P(CH_3)_3$) were determined [38] in order to investigate their potential as phosphorus source gas for n-type doping of diamond.

Chemical properties of TBP, TMP and PH_3 are summarized in table 1. The molecular structure of TBP is asymmetrical with respect to phosphorus, whereas the TMP molecular structure is symmetrical, similar to PH_3. Such structural difference is expected to produce a different decomposition and therefore a different doping incorporation ratio. TBP and TMP are usually available in liquid phase at room temperature and the vapour pressure is significantly lower than that of PH_3. Comparing the decomposition kinetics between organic (TBP and TMP) and hydride (PH_3) molecules, the most obvious difference is the lower decomposition temperature of organophosphorus. Purity, which is a key parameter in CVD growth and doping, is also shown in table 1, which indicates that hydrides are superior to organic sources.

Table 1. Chemical properties of tertiarybutylphosphine, trimethylphosphine, and phosphine.

Chemical Name	Tertiarybutylphosphine	Trimethylphosphine	Phosphine
Formula	t-P(C_4H_9)H_2	P(CH_3)$_3$	PH_3
Number of P–H bonds	2	0	3
Appearance	Colourless liquid	Colourless liquid	Colourless gas
Melting point	4.0 °C	−85 °C	−133 °C
Boiling point	56.1 °	37.8 °C	−87 °C
Toxicity (LC_{50})	∼1100 ppm 4h^{-1}	—	∼11 ppm 4h^{-1}
Explosion limit	6.4–75 vol%	—	∼1.3 vol%
Impurity content	∼1 ppm	∼1 ppm	<1 ppm (detection limit)

Such differences are expected to lead to different phosphorus incorporation ratios and/or different electronic properties, but there is almost no difference detected by SIMS, Hall-effect and cathodoluminescence analysis [38]. This indicates that for diamond growth and phosphorus doping, the plasma-induced decomposition with TBP, TMP and PH_3 is comparable, giving rise to almost the same doping properties. Usually the gas temperature is a key parameter for the molecular decomposition process. It has been reported that the gas temperature, which means neutral and ionized molecular temperatures, exceeds ∼2000 K during the CVD diamond growth [39]. The thermal decomposition of TBP was reported to start at about 800 K. It is important to note that the thermal decomposition of TMP is almost as low as TBP. Even PH_3 starts to decompose at about 1200 K [40]. The thermal decomposition temperature of these three gases is therefore much lower than the gas temperature during microwave plasma-enhanced CVD growth. Therefore, only small differences are expected, which is in agreement with our results.

The use of different source gases for phosphorus doping is summarized as follows. Since PH_3 is generally used as a source gas for phosphorus doping in Si-LSI and/or fabrication of III–V semiconductors, its purity is higher than that of organophosphorus gases. Therefore, PH_3 is favourable for high-quality doping of CVD diamond films. On the other hand, TBP and TMP are usually available in the liquid phase at room temperature and the vapour pressure is significantly lower than that of PH_3. This means that TBP and TMP have a safety advantage over PH_3 due to a toxicity level several orders of magnitude lower. However, TBP and TMP are difficult to supply with high phosphorus concentration in the gas phase because of their lower vapour phase pressure. In the present doping study of (0 0 1)-oriented diamond, PH_3 was selected as a doping gas due to its high purity and possible high phosphorus concentration.

4. Optimization for (0 0 1) phosphorus doping conditions

At the beginning, it is useful to have a first look at the conditions that prevented the successful doping of diamond. Phosphorus atoms cannot easily be incorporated into (0 0 1) facets. The efficiency is two orders of magnitude lower than the incorporation in (1 1 1)-oriented diamond. Therefore, all doping experiments failed, including polycrystalline and HTHP crystal with (0 0 1) orientation. Even in the case of partial incorporation of phosphorus, films showed very high resistivity due to co-incorporation of hydrogen along with phosphorus atoms. Hydrogen atoms are negatively charged in n-type diamond and form complexes with positively charged phosphorus donors [41]. Since such P–H complexes are electrically inactive, co-incorporation of hydrogen must be suppressed to achieve n-type conduction [42]. Moreover, growth on (1 1 1) orientation results in a smooth surface in contrast to the rough and complex surface morphologies of (0 0 1) that results in the formation of numerous hillocks. It suggests that step flow growth may not be favourable and only defective portions may act as nucleation sites for three-dimensional growth of diamond [43]. Such surface imperfections introduce deep-level defects that are also responsible for the compensation of phosphorus donors. The problem with phosphorus doping of (0 0 1) diamond can therefore be summarized as follows: (1) phosphorus has very low incorporation efficiency; (2) hydrogen will effectively terminate phosphorus and (3) additionally created defects will compensate donors.

In the case of (0 0 1) B-doped p-type diamond [44], it has been reported that the boron incorporation ratio strongly depends on the [CH_4]/[H_2] ratio and growth rate, as well as the dopant gas ratio. Boron incorporation ratio increases with an increase in growth rate. On the other hand, the density of carbon dangling bonds, which is detected by ESR, has been reported to also increase with an increase in growth rate [45]. As dangling bonds act as compensators [46], the formation of defects must be suppressed in order to realize high-quality n-type layers. This indicates that a decrease in growth rate is desirable; in fact, high-quality CVD diamond was realized by ultra-slow growth (∼3 nm h^{-1}) [14]. Phosphorus atoms will be better incorporated by high growth rate and high growth rate deposition, which unfortunately also gives rise to the incorporation of contaminants and defects. The point is that there is a trade-off between 'impurity incorporation' and 'defect suppression' against film growth rate. Taking into account this relationship, the optimization of growth parameters is one of the most important factors in achieving (0 0 1) n-type diamond.

Based on these facts, (0 0 1) phosphorus doping conditions were optimized as summarized in table 2. To suppress hydrogen co-incorporation, the substrate temperature during CVD growth was increased to ∼900 °C, which is higher than that for (0 0 1) B-doped and non-doped diamond growth. This higher substrate temperature effectively eliminated residual hydrogen atoms in the film. The substrate misorientation angle was adjusted to 2°–3°, to enhance step flow growth. In homoepitaxial growth of silicon carbide, step controlled growth is an important technique for obtaining ordered surfaces

Table 2. Typical phosphorus doping conditions for (0 0 1)-oriented diamond growth.

Source gases	PH_3, CH_4, H_2	
$[CH_4]/[H_2]$	0.4%	(0.1–1.0%)
$[PH_3]/[CH_4]$	5.0%	(1.0–25%)
Gas pressure	25 Torr	(10–100 Torr)
Total gas flow	400 sccm	
Substrate temperature	900 °C	(750–950 °C)
Substrate	Ib, IIa diamond	
Growth duration	5 h	(0.5–50 h)

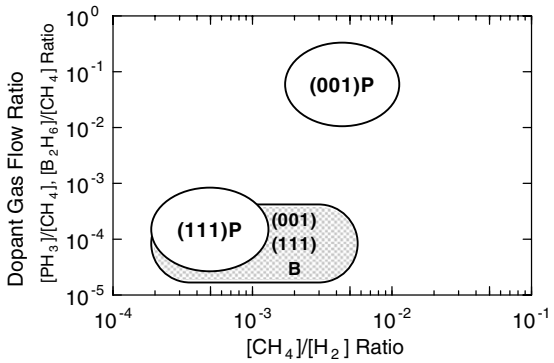

Figure 3. Parameters for phosphorus and boron doping in CVD diamond. Relationship between $[CH_4]/[H_2]$ ratio and dopant gas concentration ($[PH_3]/[CH_4]$, $[B_2H_6]/[CH_4]$). Note that all films grown under these conditions show n- or p-type conductivity in Hall-effect measurements and band conduction with thermally excited carriers from the donor or acceptor level even at room temperature.

and high crystal quality [47], so similar effects are expected for diamond growth. The main differences between (0 0 1) and (1 1 1) conditions are (1) the dilution ratio of methane, $[CH_4]/[H_2]$ and (2) the gas-phase phosphorus concentration, $[PH_3]/[CH_4]$. Figure 3 shows the differences in CVD doping conditions for both cases. The parameters for (1 1 1) phosphorus and boron doping are very similar, whereas (0 0 1)-oriented diamond requires quite different parameters. These parameters represent values that give rise to electron conduction in the conduction band, where electrons are generated by thermal excitation from a donor state. It is important to note that for an extremely high doping level ('metallic doping regime'), which results in optimized hopping conduction in the donor state, different parameters must be implemented.

Figure 4 shows typical SIMS depth profiles of (0 0 1) P-doped diamond grown under optimal conditions as described in table 2. Phosphorus atoms are clearly detected in homoepitaxial diamond films with almost uniform distribution. The incorporation efficiency, which is the ratio of [P]/[C] in the diamond film to $[PH_3]/[CH_4]$ in the gas phase ($[P]/[C]$)/($[PH_3]/[CH_4]$), is estimated at ~0.02%, which is two orders of magnitude smaller than that for phosphorus doping of (1 1 1) diamond. Basically, the other impurities are also considered to show similar orientation dependence. Boron atoms, which produce shallow acceptors located at ~0.37 eV above the valence band, and nitrogen atoms fall below the background level of SIMS measurements. Contamination with silicon and metals such as Cu, Fe and Mo is also below the

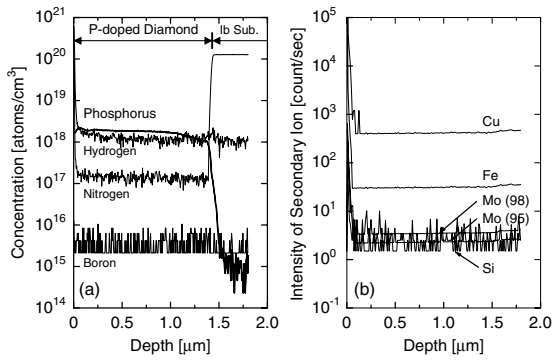

Figure 4. Typical SIMS depth profile of each element obtained for (0 0 1) P-doped diamond films grown on Ib substrate. (*a*) Atomic concentration of P, H, B and N atoms, (*b*) secondary-ion intensity of Si, Fe, Mo and Cu atoms.

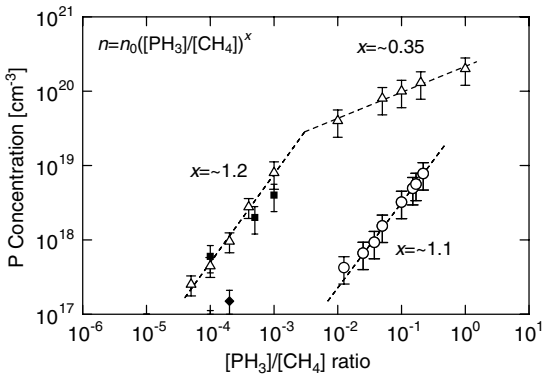

Figure 5. Changes in phosphorus concentration in (0 0 1) and (1 1 1) CVD diamond as a function of $[PH_3]/[CH_4]$ ratio. Open circles and triangles indicate the data for (0 0 1) and (1 1 1) phosphorus doping, respectively, in the present study. Closed rectangles and rhombuses are the data for (1 1 1) phosphorus doping reported by [43] and [23], respectively.

detection limit. Regarding hydrogen, it is clear from the SIMS mapping analysis that hydrogen tends to segregate in non-epitaxial crystallites in (0 0 1) P-doped diamond films [34]. In the bulk part of diamond, hydrogen also falls below the SIMS background level, which is $\sim 10^{18}$ cm^{-3}.

5. Properties of (0 0 1) and (1 1 1) P doping

The phosphorus doping properties of (0 0 1)-oriented diamond are discussed in the following, drawing comparisons with doping of (1 1 1)-oriented diamond. The phosphorus concentration in the film increases proportionally to the increase in PH_3 in the gas phase. Figure 5 shows changes in phosphorus density in the films as a function of the $[PH_3]/[CH_4]$ ratio in the gas phase. The controllable range of phosphorus concentration in (1 1 1) diamond is between $\sim 5 \times 10^{17}$ cm^{-3} and $\sim 2 \times 10^{20}$ cm^{-3}, whereas in (0 0 1) diamond it is smaller and between $\sim 5 \times 10^{17}$ and $\sim 8 \times 10^{18}$ cm^{-3}. Please note that the upper limit of $\sim 8 \times 10^{18}$ cm^{-3} is due to a safety restriction on phosphine gas usage and not due to lower incorporation efficiency. If the concentration of PH_3 in H_2 were higher, the phosphorus concentration could reach up to $\sim 10^{20}$ cm^{-3} in (1 1 1) as well. In the lower regime up to $\sim 10^{19}$ cm^{-3}, the phosphorus

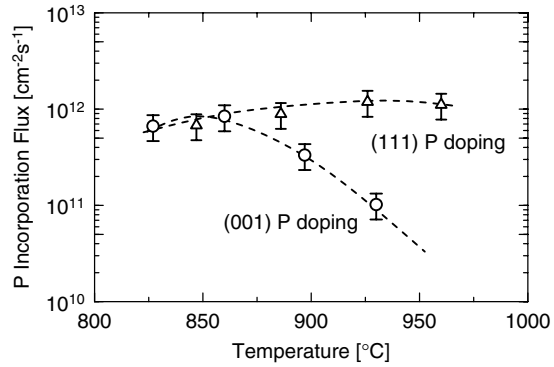

Figure 6. Temperature dependence of phosphorus incorporation flux during CVD growth. Open circles and triangles indicate the data for (0 0 1) and (1 1 1) phosphorus doping, respectively. The flux indicates the ratio of dopant atoms through the surface of the growing film per unit of square measure and time. The broken lines are guides for the eye.

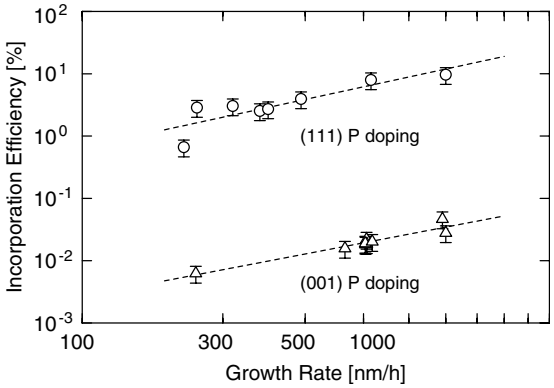

Figure 7. Relationship between growth rate and phosphorus incorporation efficiency. Open circles and triangles indicate the data for (0 0 1) and (1 1 1) phosphorus doping, respectively. The broken lines are drawn using the least-squares fit to the data.

content follows in proportion to the increase in $[PH_3]/[CH_4]$ ratio as also detected for (0 0 1) and (1 1 1) diamond. For doping higher than $\sim 10^{19}$ cm^{-3} the increase is sublinear with a gentle slope around $x \sim 0.35$. Such a tendency has also been reported for phosphorus doping of silicon [48].

Figure 6 shows the relationship between phosphorus flux and growth temperature for both (0 0 1) and (1 1 1) CVD diamond. The flux is calculated by (phosphorus concentration (cm^{-3})) × (growth ratio (cm s^{-1})), which indicates the ratio of dopant atoms through the surface of the growing film per unit area and time (cm^{-2} s^{-1}). For (1 1 1) diamond, the temperature dependence is weak, whereas for (0 0 1) diamond the flux decreases significantly with increasing growth temperature. This indicates that the thermal stability of adsorbed phosphorus atoms on the (0 0 1) diamond surface is weaker than that on (1 1 1). According to *ab initio* calculations of the absorption energy of PH_2 on (0 0 1) and (1 1 1) diamond surfaces, the energy on (0 0 1) diamond is slightly lower than that on (1 1 1) [49]. This is in agreement with the presented experimental results and also provides one of the reasons for the lower incorporation efficiency of (0 0 1) diamond.

Figure 7 shows the relationship between phosphorus incorporation efficiency and growth rate in both (0 0 1) and (1 1 1) antimony doping. The absolute values are quite different, but the slopes are similar. This is consistent with *ab initio* calculations of phosphorus doping [50]. The phosphorus atoms tend to segregate towards the surface, and this tendency is stronger in (0 0 1) than in (1 1 1) diamond. In other words, phosphorus atoms are more difficult to incorporate on a (0 0 1) surface than on (1 1 1). Therefore, the doping efficiency on (0 0 1) is lower than that on (1 1 1). To overcome this problem, it is necessary to grow diamond at a faster rate than the surface segregation velocity of phosphorus atoms. Therefore, a higher growth rate leads to higher incorporation efficiency. This has been pointed out in antimony doping of silicon [51].

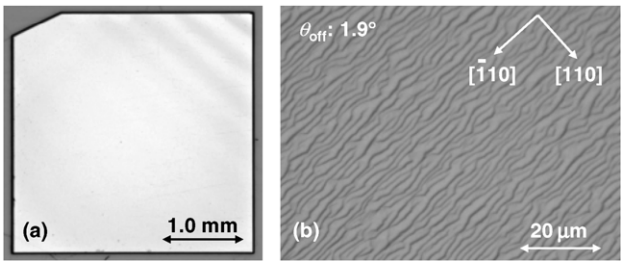

Figure 8. Typical surface morphology obtained for (0 0 1) P-doped diamond grown on Ib substrate with misorientation angle of ∼1.9°. (*a*) Optical microscope image, (*b*) differential interference microscope with Nomarski prism.

6. Characterization of surface morphology and crystallinity

Figure 8 shows a typical surface morphology of (0 0 1) P-doped diamond film grown on Ib substrate with a misorientation angle of ∼1.9°. The periodic structure is not due to macroscopic substrate surface roughness caused by polishing, but rather to microscopic growth kinetics, as the direction of the periodic structure is along a specific crystal orientation, giving rise to 'step bunching'. The entire surface is covered with these steps, the height of which was estimated by atomic force microscopy at between ∼20 and ∼50 nm. The average roughness of each terrace is ∼0.5 nm. Non-epitaxial crystallites and pyramidal hillocks, which are often seen on (0 0 1) homoepitaxial CVD diamond, were partially detected. This morphology strongly depends on the substrate misorientation angle θ_{off}. Towards lower θ_{off}, the density of non-epitaxial crystallites and pyramidal hillocks increases, leading to a degradation of surface properties. Increase in misorientation angle to 2°–3° is necessary for uniform phosphorus doping of (0 0 1)-oriented diamond.

Figure 9 shows the XRD rocking curves of the (0 0 4) diffraction obtained for thick (0 0 1) P-doped diamond, grown on IIa substrate with a misorientation angle of ∼2.3°. The full width at half maximum (FWHM) for the CVD film was estimated at ∼11.5 arcsec given by the average of 20 measurements from arbitrary locations of the sample, which is almost comparable to that of HTHP synthetic IIa substrate of ∼10 arcsec. This indicates that the crystal perfection of the present (0 0 1) diamond is good, although the slight broadening of FWHM obtained in XRD and Raman analyses might be due to expansion of the lattice constant by phosphorus doping.

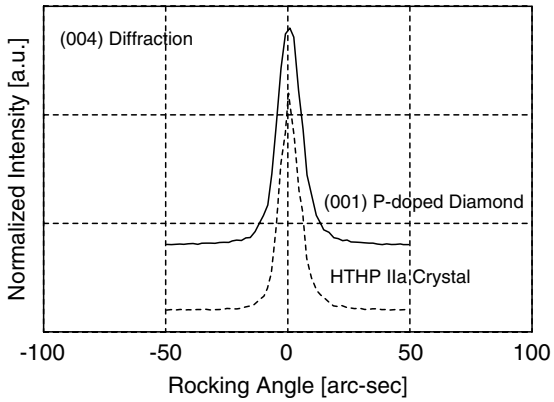

Figure 9. XRD rocking curves obtained for thick (0 0 1) P-doped diamond grown on IIa substrate with misorientation angle of ∼2.3° (solid curve) and for IIa substrate only (broken curve). The FWHM of (0 0 4) reflection spectrum was estimated using the average of 20 measurements from arbitrary locations of the sample.

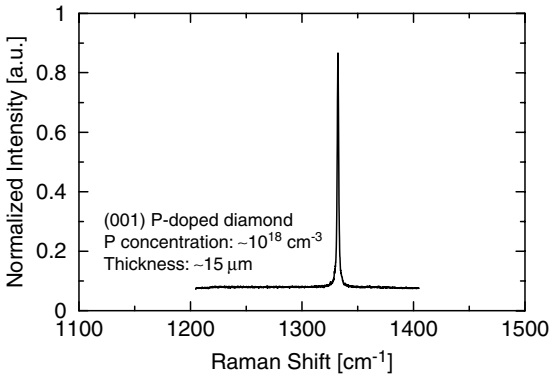

Figure 10. Raman spectrum obtained for thick (0 0 1) P-doped diamond grown on IIa substrate with a misorientation angle of ∼2.3°. (Excited by Ar laser: 514 nm.)

Figure 10 shows the Raman spectrum obtained for the same sample by Ar laser (514 nm). A sharp symmetric diamond peak at 1332.5 cm^{-1} with FWHM of ∼1.86 cm^{-1} was detected without other spectral components from the non-diamond phase. The peak width is consistent with that of the reported (1 1 1) P-doped diamond [43]. No shift was observed in the peak position between P-doped diamond and HTHP synthetic IIa crystal, but there was a slight broadening of the FWHM, which seems to be consistent with the XRS results. The strain-induced broadening could have occurred due to the size mismatch between phosphorus and carbon. Further characterization is needed for a more detailed discussion.

Macroscopic crystallinity and surface smoothness were determined by RHEED analysis. The RHEED patterns in the [1 0 0] and [1 1 0] directions obtained for a hydrogen-terminated surface of (0 0 1) P-doped diamond grown on Ib substrate with a misorientation angle of ∼1.9° are shown in figures 11(*a*) and (*b*), respectively. The incidence angle of the electron beam was chosen to fit the (0 0 4) Bragg condition at ∼2°. Sharp Kikuchi patterns with low background were observed as bulk diffraction effects due to inelastically scattered electrons from the bulk. In the case of a rough surface, these inelastically scattered electrons can barely reach the vacuum without scattering, which would result in the

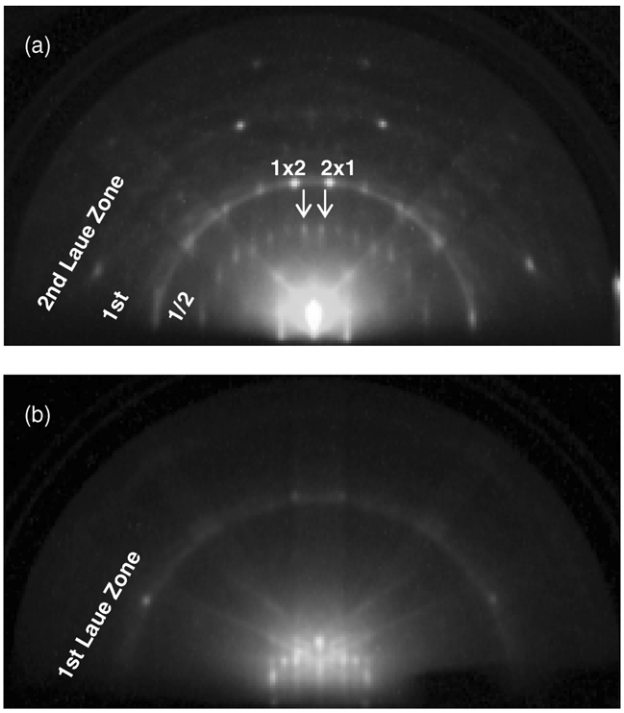

Figure 11. RHEED patterns in the [1 0 0] direction (*a*) and [1 1 0] direction (*b*), obtained for hydrogen-terminated surface of (0 0 1) P-doped diamond grown on Ib substrate with a misorientation angle of ∼1.9°. The incident angle of the electron beam is under the (0 0 4) Bragg condition at approximately 2°. Electron beam energy: 20 keV.

disappearance of Kikuchi patterns. Moreover, fine streaks due to the ordered surface and sharp bulk spots were observed in the zeroth-order Laue zone. These RHEED patterns indicate that the surface smoothness and crystallinity of the present (0 0 1) P-doped diamond film are good. Moreover, surface spots corresponding to a $2 \times 1/1 \times 2$ double-domain structure were observed in the half-order Laue zone in figure 11(*a*). Since the $2 \times 1/1 \times 2$ reconstruction is typical in (0 0 1) H-terminated diamond surfaces, the grown P-doped diamond surface can be confirmed as being (0 0 1) oriented.

7. Electrical conduction properties

Hall-effect measurement is the most straightforward method for characterizing the electrical conduction mechanisms in semiconductors. We therefore performed a series of temperature dependent Hall-effect measurements on all P-doped diamond films. Figure 12 shows typical results of carrier concentrations obtained for (0 0 1) and (1 1 1) P-doped diamond films. Circles and rectangles indicate phosphorus-doped (0 0 1)-oriented diamond with $\sim 2 \times 10^{18}$ cm^{-3} and $\sim 6 \times 10^{17}$ cm^{-3} phosphorus, respectively. Triangles are typical results on (1 1 1) diamond with $\sim 2 \times 10^{18}$ cm^{-3} phosphorus. These films show n-type Hall signals, indicating n-type conductivity over a wide temperature range from room temperature to 1000 K. This is common to all films grown under the conditions shown in figure 3. The electron concentration increases exponentially with increasing temperature. This indicates that the carrier conduction is

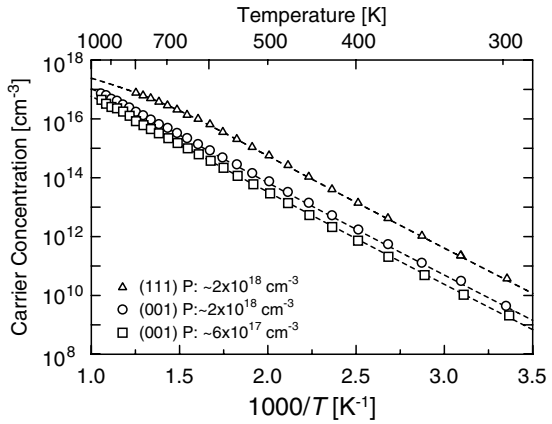

Figure 12. Temperature dependence of carrier concentration of P-doped diamond films obtained by Hall-effect measurements. Circles, rectangles and triangles indicate the data for (0 0 1) P-doped diamond with phosphorus concentration of $\sim 2 \times 10^{18}$ cm^{-3}, (0 0 1) with phosphorus concentration of $\sim 6 \times 10^{17}$ cm^{-3} and (1 1 1) with phosphorus concentration of $\sim 2 \times 10^{18}$ cm^{-3}, respectively. Each broken line is the least-squares fit to the data, applying equation (3).

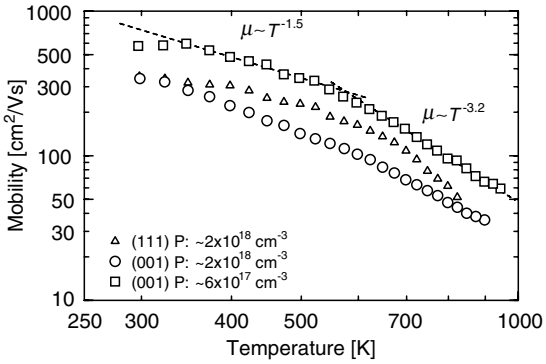

Figure 13. Temperature dependence of carrier mobility of P-doped diamond films. Circles, rectangles and triangles indicate the data for (0 0 1) P-doped diamond with phosphorus concentration of $\sim 2 \times 10^{18}$ cm^{-3}, (0 0 1) with phosphorus concentration of $\sim 6 \times 10^{17}$ cm^{-3} and (1 1 1) with phosphorus concentration of $\sim 2 \times 10^{18}$ cm^{-3}, respectively. The broken lines are drawn using the least-squares fit to the data for acoustic phonon scattering ($\mu \sim T^{-1.5}$) and others ($\mu \sim T^{-3.2}$).

dominated by free electrons in the conduction band, which is thermally activated from the donor level.

The electron concentration, n, can be calculated by taking into account the donor states, N_{D}, and compensating acceptor states, N_A, which may originate from impurity atoms and/or defects:

$$\frac{n(n+N_{\mathrm{A}})}{N_{\mathrm{D}}-N_{\mathrm{A}}-n} = \frac{N_{\mathrm{C}}}{g}\exp\left(-\frac{E_{\mathrm{D}}}{k_{\mathrm{B}}T}\right), \qquad (1)$$

where k_{B} is the Boltzmann constant, T is the temperature, g is the degeneration of the donor level E_{D} (=2 for diamond) and N_{C} is the effective density of states in the conduction band as expressed by the following:

$$N_{\mathrm{C}} = 2M_{\mathrm{C}}\left(\frac{2\pi m^*_{\mathrm{dos}}k_{\mathrm{B}}T}{h^2}\right), \qquad (2)$$

where M_{C} is the number of equivalent minima in the conduction band (=6 for diamond) and h is the Planck constant. The density-of-state effective mass of electrons m^*_{dos} is given by $m^*{}_{\mathrm{dos}} = (m^*_{\mathrm{l}}m^*_{\mathrm{t}}m^*_{\mathrm{t}})^{1/3}$, where m^*_{l} and m^*_{t} are the longitudinal and transverse effective mass of electrons, respectively. We assumed $m^*_{\mathrm{l}} = 1.4m_0$ and $m^*_{\mathrm{t}} = 0.36m_0$, where m_0 is the free electron mass [52].

In the temperature region in which n is significantly lower than N_{A} and N_{D}, i.e. $n \ll N_{\mathrm{A}} < N_{\mathrm{D}}$, equation (1) is simplified using the compensation ratio $\eta = N_{\mathrm{A}}/N_{\mathrm{D}}$,

$$n = \frac{1-\eta}{\eta}\frac{N_{\mathrm{C}}}{g}\exp\left(-\frac{E_{\mathrm{D}}}{k_{\mathrm{B}}T}\right). \qquad (3)$$

E_{D} and η can be easily estimated from a least-squares fit to the data using equation (3). The broken lines shown in figure 11 are the least-square fit as calculated by equation (3). The value of E_{D} for all films is 0.56–0.58 eV and is equal to the results reported for (1 1 1) P-doped diamond [23]. The compensation ratio, $\eta = N_{\mathrm{A}}/N_{\mathrm{D}}$, of (0 0 1) diamond is about ~54% for phosphorus concentration of $\sim 2 \times 10^{18}$ cm^{-3} and ~66% for $\sim 6 \times 10^{17}$ cm^{-3}, which is about one order of magnitude higher than in (1 1 1) diamond (~7%).

Figure 13 shows typical temperature-dependent variations in mobility obtained for (0 0 1) and (1 1 1) diamond films. Circles, rectangles and triangles indicate data for (0 0 1) P-doped diamond with phosphorus concentration of $\sim 2 \times 10^{18}$ cm^{-3} and $\sim 6 \times 10^{17}$ cm^{-3} and for (1 1 1) with a phosphorus concentration of $\sim 2 \times 10^{18}$ cm^{-3}, respectively. At room temperature, comparable mobility of ~350 cm^2 V^{-1} s^{-1} can be detected in (0 0 1) and (1 1 1) P-doped diamond with almost similar phosphorus concentration of $\sim 2 \times 10^{18}$ cm^{-3}. It is interesting to note that until now, the defect compensation in (0 0 1) diamond was higher than in (1 1 1). Despite this fact, the mobility in one of the films at 300 K was equal to the (1 1 1) film. In addition, towards lower phosphorus concentrations, the mobility at room temperature increased up to ~570 cm^2 V^{-1} s^{-1}.

From the temperature dependence features, the electron mobility in all films is considered to be dominated by phonon or intervalley scattering. Towards higher temperatures ($T >$ 500 K), the mobility becomes steeper than $\mu \propto T^{-1.5}$ (acoustic phonon scattering). Towards lower temperatures at around room temperature, the dependence of μ in all films deviates from the effect of acoustic phonon scattering. The films are strongly compensated, pointing towards a non-negligible defect density that can be ionized, giving rise to the observed decrease of μ, although some ambiguity may exist in the mobility measurements due to the contribution of hopping conduction.

This trend of temperature dependence of μ obtained for (0 0 1) P-doped diamond is almost the same as that reported for (1 1 1). The highest mobility achieved up to now was ~570 cm^2 V^{-1} s^{-1} ($P \sim 6 \times 10^{17}$ cm^{-3}) for (0 0 1) and ~660 cm^2 V^{-1} s^{-1} ($P \sim 7 \times 10^{16}$ cm^{-3}) for (1 1 1) [23]. These values are, however, much lower than that reported for high-quality B-doped diamond films: ~1800 cm^2 V^{-1} s^{-1} ($B \sim 6 \times 10^{17}$ cm^{-3}) at room temperature [15]. On one side, the higher carrier compensation ratio could be one of the reasons. On the other side, the effects of native defects and/or

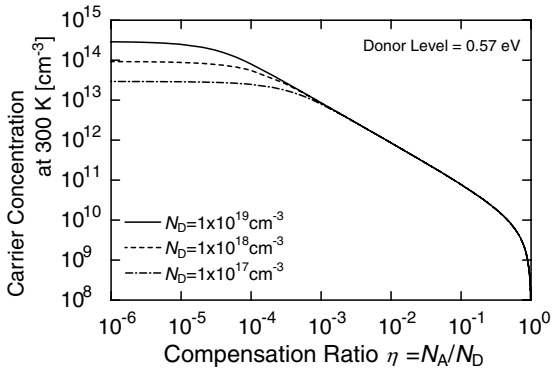

Figure 14. Relationship between the carrier concentration at room temperature and the compensation ratio, theoretically calculated for various N_D of 1×10^{17}, 1×10^{18} and 1×10^{19} cm^{-3} with donor level of 0.57 eV by equations (1) and (2).

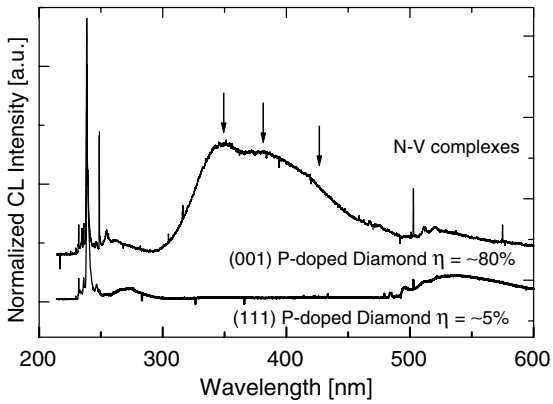

Figure 15. Cathodoluminescence spectra obtained at 16 K for (0 0 1) phosphorus-doped diamond with high compensation ratio η of ∼80% and (1 1 1) with η of ∼5%. Spectra were normalized by the peak intensity of phosphorus bound-exciton emission with transverse optical phonons.

structural distortion due to the incorporation of phosphorus atoms may be another reason for the lower mobility of P-doped diamond.

8. Carrier compensation in (0 0 1) P-doped diamond

To attain a more thorough understanding of the electrical conduction properties, the following discussion focuses on the effect of carrier compensation due to impurities and/or defects. Figure 14 shows changes in carrier concentration at room temperature as a function of compensation ratio η calculated using equations (1) and (2) with a donor level of 0.57 eV and donor density between N_D of 1×10^{17}, 1×10^{18} and 1×10^{19} cm^{-3}. The electron concentration at room temperature is approximately 10^9–10^{14} cm^{-3} due to the deep donor level of phosphors. The electron concentration decreases significantly with an increase in compensation centres, while it is insensitive to the N_D values. This characteristic, called 'deep dopant effect', has been discussed by Koide [53]. Therefore, for P-doped diamond, improvement of electrical properties requires the reduction of compensating defects rather than the increase in donor concentration.

Until now, however, the clear identification of compensating centres has been difficult. Unintentionally incorporated boron atoms in films are one candidate for compensation centres. For the samples used here, however, boron could not be detected by SIMS, as shown in figure 3. Other elements such as N, Si, Cu, Fe and Mo also could not be detected. One possibility would be the phosphorus–vacancy (P–V) complexes suggested by Jones *et al* [54]. Here, phosphorus lies at the midpoint between two neighbouring vacancies. This complex introduces an acceptor state ∼2.7 eV below the conduction band. In addition, the estimated binding energy of the P–V complex is ∼7.1 eV for dissociation into neutral constituents, which is much larger than that of the P–H complex of ∼2.6 eV, indicating that the P–V complex is more stable in P-doped diamond [55]. Actually, the compensation centres, calculated by assuming that donor concentration is equal to phosphorus concentration, increase with an increase in phosphorus concentration [56]. If some of the incorporated phosphorus atoms in (0 0 1)-oriented diamond induce such P–V complexes, it would explain the detected features.

On the other hand, H1′ centres, often observed in CVD diamond by ESR, are another candidate for donor compensation [43]. H1' centres are possibly hydrogen–vacancy complexes, where the carbon dangling bond is near a hydrogen atom. Since this defect is observed not only in non-doped but also in B-doped CVD diamond, it has been suggested that its electronic state, D(0/+), lies between the valence band top and boron acceptor level [57]. However, in (0 0 1) P-doped diamond, such defects were not observed by ESR. This result indicates two possibilities: (1) these defects are not generated in n-type diamond, and (2) the defects of H1′ centres are generated even in n-type diamond, but their charge is changed from D(0/+) to D(−/0) by compensating donor electrons, where the D(−/0) state is located below the phosphorus donor level and therefore cannot be detected by ESR analysis.

Cathodoluminescence analysis is a well-known technique used to characterize defects and impurity effects for diamond with high sensitivity. Figure 15 shows typical cathodoluminescence spectra at 16 K obtained for (0 0 1) and (1 1 1) P-doped diamond films. Each spectrum was normalized by the peak intensity of phosphorus bound-exciton emission with transverse optical phonons. In the near-band-edge region, strong sharp excitonic emission lines were clearly observed regardless of the substrate orientation. All peaks were almost identical to those previously reported for (1 1 1) P-doped diamond films [58]. The peak at ∼5.27 eV is due to the free-exciton emission associated with a transverse optical phonon (FE_{TO}). Referring to the results of (1 1 1) P-doped diamond, all peaks in the near-band-edge region are due to P-donor bound-exciton (P-BE) emission with each phonon. From the observation of P-BE emission, it was confirmed that incorporated phosphorus atoms are located in substitutional sites in the diamond lattice as donor atoms. On the other hand, there are clear differences in the range from 300 to 500 nm. Broad peaks with ∼350, ∼380 and ∼430 nm are clearly seen in (0 0 1) P-doped diamond. The band around ∼430 nm is referred to as 'Band-A emission' due to the structural dislocation [59]. The broad bands around ∼350 and ∼380 nm often appear in electroluminescence spectra of polycrystalline diamond films and homoepitaxial p–n junctions [60, 61].

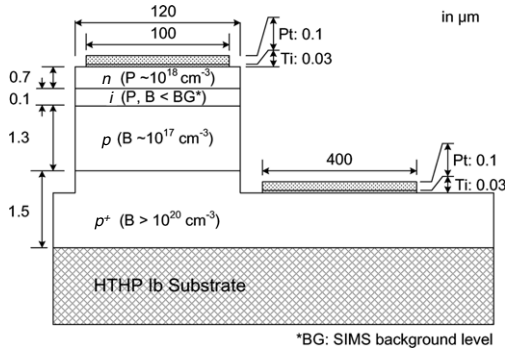

Figure 16. Schematic diagram of p–i–n junction diode fabricated by CVD on (0 0 1)-oriented Ib diamond substrate. Boron and phosphorus concentrations were controlled at $\sim 3 \times 10^{20}$ cm^{-3}, $\sim 2 \times 10^{17}$ cm^{-3} and $\sim 1 \times 10^{18}$ cm^{-3} for p$^+$, p and n-type layers, respectively. For intrinsic layers, the impurity concentration was below the SIMS background level. The thickness of p+, p, intrinsic, and n-type layers was controlled at $\sim 1.5\,\mu$m, 1.3 μm, 0.1 μm and 0.7 μm, respectively. Diameter of the mesa structure is 120 μm. Ti (30 nm)/Pt (100 nm) electrodes with 100 μm and 400 μm were used on n- and p$^+$-type layers, respectively.

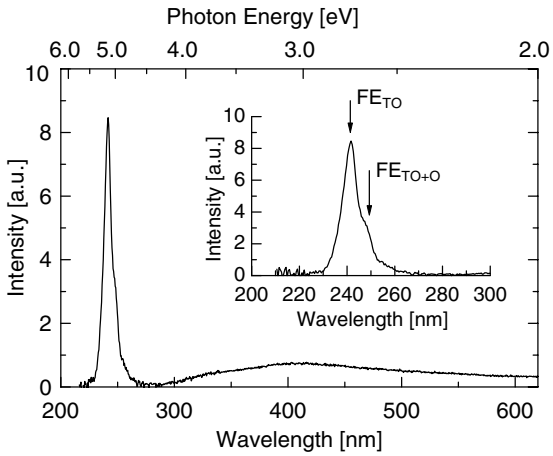

Figure 17. Current injected light emission spectrum of p–i–n junction at room temperature. The spectrum was obtained under a current of $\sim$79 mA at a voltage of 30 V. The inset shows the spectrum expanded around the near-band-edge region.

Although there is no assignation of their physical nature, they could correspond to the phosphorus incorporation in the diamond lattice. It is also expected that these emission bands correspond to compensation centres such as P–V complexes or H1′ centres as mentioned above. Further investigation by CL and ESR detailed analysis will identify the origin of defects compensating phosphorus donors.

9. Excitonic emission from (0 0 1) p–i–n junction diode

Deep UV light sources with a wavelength shorter than 350 nm have attracted much research interest because of their potential applications in biochemical detection, high-density data storage and air-water purification. Diamond is one of the attractive candidates for UV light emitting applications because of its wide-band-gap energy of 5.5 eV. The large exciton binding energy of around 80 meV and small Bohr radius of 1.57 nm due to its lower dielectric constant represent the high-density storage of excitons around 10^{18}–10^{19} cm^{-3} even at room temperature [12]. This unique advantage is considered to be utilized for high-efficiency deep UV light source, which would be comparable to other luminescent direct-transition semiconductors emitting light by free electron–hole recombination such as III–V compounds. In this study, based on the present achievement of (0 0 1) n-type diamond growth, high-quality p–i–n junction was fabricated on (0 0 1)-oriented diamond substrate, and UV light emission of around 240 nm was demonstrated even at room temperature [3, 35].

Figure 16 shows a schematic diagram of the p–i–n junction device structure. Each impurity was controlled at $\sim 3 \times 10^{20}$ cm^{-3} of boron atoms for p$^+$-type layers and $\sim 2 \times 10^{17}$ cm^{-3} for p-type layers and $\sim 1 \times 10^{18}$ cm^{-3} of phosphorus atoms for n-type layers. For intrinsic layers, phosphorus and boron concentrations were below the SIMS background levels. The thickness of p$^+$, p, intrinsic and n-type layers was controlled at $\sim 1.5\,\mu$m, 1.3 μm, 0.1 μm and 0.7 μm, respectively. Please note that all the layers here were grown by CVD, which is unusual for this junction device. Mesa structures with an area of 120 μm diameter were fabricated by conventional photolithography and inductively coupled plasma etching process in order to reduce the leakage current. Ti (30 nm)/Pt (100 nm) electrodes with 100 μm and 400 μm were formed on n- and p$^+$-type layers, respectively, and then were annealed at 420 °C for 30 min in Ar ambient atmosphere. For n-type layers, Ti contact did not show perfect ohmic current–voltage characteristics. Usually in (1 1 1) n-type diamond, heavily P-doped layers with phosphorus concentration exceeding $\sim 10^{19}$ cm^{-3} is introduced under the electrodes in order to form ohmic contact [62], whereas heavy doping is yet be reached in (0 0 1) P-doped diamond (see figure 4). The development of good ohmic contact is the next key subject for n-type diamond research.

The electric properties of p–i–n junction devices were examined by current–voltage and capacitance–voltage measurements, the results of which provided clear diode characteristics with a rectification ratio of about 10^{10} at ± 25 V [3]. At forward current exceeding $\sim 5\,\mu$A, visible light emission started, and then UV light emission was observed above $\sim$6 mA. Figure 17 shows a typical light emission spectrum of the p–i–n junction device observed at room temperature. The spectrum was obtained by forward carrier injection under a current of $\sim$79 mA at a voltage of 30 V. Strong, sharp UV emission with a peak wavelength of $\sim$240 nm, which is attributed to FE_{TO} and its phonon replica ($FE_{TO+\Gamma O}$), can be clearly observed. The UV emission intensity increases strongly with an increase in the forward carrier injection. The origin of visible emission has not yet been clarified, although it is considered to be related to n-type layer defect states, as shown in figure 15. What is significant in the present demonstration as shown in figure 16 is that UV emission intensity (I_{FE}) is considerably higher than the emission due to deep levels (I_{deep}). The relative integrated intensity (I_{FE}/I_{deep}) improves up to 0.55, which is one order of magnitude higher than that of our previous results [35] and that reported for diamond p–n junction devices [2, 9]. Such developments are indicative of the significant improvement

in electronic quality in single-crystal CVD diamond layers, and represent a major step toward the realization of viable electronic devices. By further optimizing each CVD layer, more efficient UV light emission would be attained, leading to future optoelectronics applications such as biochemical detection, data storage and air-water purification.

10. Summary

n-type doping of (0 0 1)-oriented diamond, one of the most challenging targets of diamond growth, was achieved by phosphorus doping using a MPCVD technique and optimized growth parameters. n-type conductivity and incorporation of phosphorus were confirmed using Hall-effect and SIMS measurements, respectively. A sharp symmetric diamond peak without other spectral components from non-diamond phases was obtained in XRD rocking curves of (0 0 4) diffraction and Raman spectroscopy analyses. The observation of diffraction spots, streaks and Kikuchi patterns in reflection high-energy electron diffraction analysis indicate high surface smoothness and good crystallinity quality. Since the 2×1 reconstruction is typical in a (0 0 1) H-terminated diamond surface, the grown P-doped diamond surface was confirmed as being (0 0 1) oriented. The observation of EF and P-BE emissions revealed that the crystal perfection is relatively fine and phosphorus atoms are located in substitutional sites of the diamond lattice as donor atoms.

Detailed properties of phosphorus doping of (0 0 1)-oriented diamond were investigated and compared with (1 1 1)-oriented diamond. The data shows that the phosphorus incorporation efficiency has a clear dependence on growth rate. Higher growth rate leads to higher incorporation efficiency of phosphorus atoms regardless of substrate orientation. However, the total value of incorporation efficiency of (0 0 1)-oriented diamond is two orders of magnitude lower than that of (1 1 1)-oriented diamond. Until now, a carrier concentration regime between $\sim 5 \times 10^{17}$ and $\sim 8 \times 10^{18}\,\mathrm{cm}^{-3}$ could be reproducibly achieved. From Hall-effect and conductivity data, the carrier compensation ratio of (0 0 1)-oriented diamond is rather high, namely about 50%. In spite of such a compensation ratio, high mobility of $\sim 570\,\mathrm{cm}^2\,\mathrm{V}^{-1}\,\mathrm{s}^{-1}$ was achieved for (0 0 1) diamond with a phosphorus concentration of $\sim 6 \times 10^{17}\,\mathrm{cm}^{-3}$.

Based on the present achievement of (0 0 1) n-type diamond growth, p–i–n junction diode was fabricated on (0 0 1)-oriented diamond substrate, and high-efficiency exciton emission with deep UV light around 240 nm was realized by carrier injection even at room temperature. The relative integrated intensity of UV light to deep levels reached 0.55 at a forward current of ~ 79 mA.

Phosphorus for n-type doping of (1 1 1)- and (0 0 1)-oriented diamond has finally been achieved nearly 10 years after the discovery of phosphorus doping. This was one of the most important successes bringing diamond closer to electronic applications. Future research activities will focus on the realization of metallically doped diamond ($>10^{20}\,\mathrm{cm}^{-3}$) and on ohmic and Shottky contact optimization. As the phosphorus level is relatively deep in the band gap of diamond, high-temperature electronic applications will also be a main target. Whether diamond will become a major part of future electronics ultimately depends on the availability of large diamond substrates for homoepitaxial growth.

Acknowledgments

This work was partly supported by the New Energy and Industrial Technology Development Organization and the Sumitomo Foundation 2006 (Grant for Basic Science Research Projects). We sincerely thank Dr C E Nebel of the Diamond Research Center at AIST, Dr S Koizumi of the Advanced Materials Laboratory at NIMS, Dr T Miyazaki of the Research Institute for Computational Sciences at AIST and all the members of the High Temperature Quantum Electronics (HTQE) Group of the Nanotechnology Research Institute at AIST for their valuable advice, encouragement and discussions. Please note that the present UV-LED device was realized by the many efforts of the HTQE group members. Appreciation is also extended to Dr M Hasegawa of the Research Center for Advanced Carbon Materials at AIST for his help in Hall-effect measurement, Dr M Nishizawa of the Advanced Semiconductor Research Center at AIST for RHEED analysis and Dr H Watanabe of the Diamond Research Center at AIST for CL analysis.

References

[1] Collins A T and Lightowler E C 1979 *The Properties of Diamond* ed J E Field (London: Academic)
[2] Koizumi S, Watanabe K, Hasegawa M and Kanda H 2001 *Science* **292** 1899–901
[3] Makino T, Tokuda N, Kato H, Ogura M, Watanabe H, Ri S G, Yamasaki S and Okushi H 2006 *Japan. J. Appl. Phys.* **45** L1042–44
[4] Hayashi K, Tachibana T, Kawakami N, Yokota Y, Kobashi K, Ishihara H, Uchida K, Nippashi K and Matsuoka M 2006 *Diamond Relat. Mater.* **15** 792–96
[5] Ono T, Sakai T, Sakuma N, Suzuki M, Yoshida H and Uchikoga S 2006 *Diamond Relat. Mater.* **15** 1998–2000
[6] Suzuki M, Koizumi S, Katagiri M, Ono T, Sakuma N, Yoshida H, Sakai T and Uchikoga S 2006 *Phys. Status Solidi.* a **203** 3128–35
[7] Yamada T, Nebel C, Rezek B, Takeuchi D, Fujimori N, Namba A, Nishibayashi Y, Yamaguchi H, Saito I and Okano K 2005 *Appl. Phys. Lett.* **87** 234107-1-3
[8] Umezawa H, Tokuda N, Ogura M, Ri S G and Shikata S 2006 *Diamond Relat. Mater.* **15** 1949–53
[9] Horiuchi K, Kawamura A, Ide T, Ishikura T, Nakamura K and Yamashita S 2001 *Japan. J. Appl. Phys.* **40** L275–8
[10] Kasu M, Ueda K, Ye H, Yamauchi Y, Sakai S and Makitnoto T 2005 *Electron. Lett.* **41** 1249–50
[11] Hasegawa M, Takeuchi D, Yamanaka S, Ogura M, Watanabe H, Kobayashi N, Okushi H and Kajimura K 1999 *Japan. J. Appl. Phys.* **38** L1519–22
[12] Okushi H, Watanabe H, Yamasaki S and Kanno S 2006 *Phys. Status Solidi.* a **203** 3226–44
[13] Watanabe H and Okushi H 2000 *Japan. J. Appl. Phys.* **39** L835–7
[14] Kamo M, Sato Y, Matsumoto S and Setaka N 1983 *J. Cryst. Growth* **62** 642–4
[15] Yamanaka S, Watanabe H, Masai S, Takeuchi D, Okushi H and Kjimura K 1998 *Japan. J. Appl. Phys.* **37** L1129–31
[16] Chen Y G, Ogura M and Okushi H 2003 *Appl. Phys. Lett.* **82** 4367–9
[17] Teraji T 2006 *Phys. Status Solidi* a **203** 3324–57
[18] Koizumi S, Kamo M, Sato Y, Ozaki and Inuzuka T 1997 *Appl. Phys. Lett.* **71** 1065–7

[19] Kato H, Futako W, Yamasaki S and Okushi H 2004 *Diamond Relat. Mater.* **13** 2117–20
[20] Nesladek M 2005 *Semicond. Sci. Technol.* **20** R19–27
[21] Tajani A, Gheeraert E, Casanova N, Bustarret E, Garrido J A, Rumen G, Nebel C E, Newton M E and Evans D 2002 *Phys. Status Solidi* a **193** 541–5
[22] Kociniewski T *et al* 2006 *Phys. Status Solidi* a **203** 3136–41
[23] Katagiri M, Isoya J, Koizumi S and Kanda H 2004 *Appl. Phys. Lett.* **85** 6365–7
[24] Isberg J, Hammersberg J, Johansson E, Wikström T, Twitchen D J, Whitehead A J, Coe S E and Scarsbook G A 2002 *Science* **297** 1670–2
[25] Farrer R 1969 *Solid State Commun.* **7** 685
[26] Orita N, Nishimatsu T and Yoshida H K 2007 *Japan. J. Appl. Phys.* **46** 315–7
[27] Kajihara S A, Antonelli A, Bernholc J and Car R 1991 *Phys. Rev. Lett.* **66** 2010–3
[28] Goss J P, Briddon P R, Jones R and Sque S 2004 *Diamond Relat. Mater.* **13** 684–90.
[29] Lombardi E B, Mainwood A and Osuch K 2004 *Phys. Rev.* B **70** 205201-1-12
[30] Sque S J, Jones R, Goss J P and Briddon P R 2004 *Phys. Rev. Lett.* **92** 017402-1-4
[31] Katagiri M, Isoya J, Koizumi S and Kanda H 2006 *Phys. Status Solidi* a **203** 3367–74
[32] Isoya J, Katagiri M, Umeda T, Koizumi S, Kanda H, Son N T, Henry A, Gali A and Janzén E 2006 *Physica* **376–377** 358–61
[33] Kato H, Yamasaki S and Okushi H 2005 *Appl. Phys. Lett.* **86** 222111-1-3
[34] Kato H, Watanabe H, Yamasaki S and Okushi H 2006 *Diamond Relat. Mater.* **15** 548–53
[35] Makino T, Kato H, Ogura M, Watanabe H, Ri S G, Yamasaki S and Okushi H 2005 *Japan. J. Appl. Phys.* **44** L1190–92
[36] Pearse R W B P and Gaydon A G 1976 *The Identification of Molecular Spectra* 4th edn (London: Chapman and Hall)
[37] Takeuchi D, Yamanaka S, Watanabe H, Sawada S, Ichinose H, Okushi H and Kajimura K 1999 *Diamond Relat. Mater.* **8** 1046–9
[38] Kato H, Yamasaki S and Okushi H 2005 *Phys. Status Solidi* a **202** 2122–8
[39] Hassouni K, Grotjohn T A and Gicquel A 1999 *J. Appl. Phys.* **86** 134–51
[40] Larsem C A, Buchan N I and Stringfellow G B 1987 *J. Cryst. Growth* **85** 148–53
[41] Goss J P, Jones R, Heggie M I, Ewels C P, Briddon P R and Öberg S 2002 *Phys. Rev.* B **65** 115207-1-13
[42] Wang L G and Zunger A 2002 *Phys. Rev.* B **66** 161202-1-4
[43] Koizumi S 1999 *Phys. Status Solidi* a **172** 71–8
[44] Ogura M, Chen Y G, Ri S G, Watanabe H, Yamasaki S and Okushi H 2004 *15th Eur. Conf. on Diamond, Diamond-Like Materials, Carbon Nanotubes, Nitrides & Silicon Carbide (Diamond 2004)* article 11.5
[45] Mizuochi N, Watanabe H, Okushi H, Yamasaki S, Niitsuma J and Sekiguchi T 2006 *Appl. Phys. Lett.* **88** 091912-1-3
[46] Zhou X, Watkins G D, Rutledge K M M, Messmer R P and Chawla S 1996 *Phys. Rev.* B **54** 7881–90
[47] Ueda T, Nishino H and Matsunami H 1990 *J. Cryst. Growth* **104** 695–700
[48] Mehta B and Tao M 2005 *J. Electrochem. Soc.* **152** G309-15
[49] Larsson K 2003 *Comput. Mater. Sci.* **27** 23–9
[50] Miyazaki T, Kato H, Ri S G, Ogura M, Tokuda N and Yamasaki S 2006 *Superlatt. Microstruct.* **40** 574–9
[51] Jorke H 1988 *Surf. Sci.* **193** 569–78
[52] Nava F, Canali C, Jacoboni C, Reggiani L and Kozlov S F 1980 *Solid State Commun.* **33** 475–7
[53] Koide Y 2004 *Japan. J. Appl. Phys.* **43** 3307–10
[54] Jones R, Lowther J E and Goss J 1996 *Appl. Phys. Lett.* **69** 2489–91
[55] Miyazaki T and Yamasaki S 2006 *Physica* B **376–377** 304–6
[56] Kato H, Yamasaki S and Okushi H 2007 *Diamond Relat. Mater.* **16** 796–9
[57] Mizuochi N, Ogura M, Watanabe H, Isoya J, Okushi H and Yamasaki S 2004 *Diamond Relat. Mater.* **13** 2096–9
[58] Sauer R, Teofilov N, Thonke K and Koizumi S 2004 *Phys. Status Solidi* a **201** 2405–13
[59] Dean P J 1965 *Phys. Rev.* **139** A588–602
[60] Wada M, Kadri M, Bustarret E, Deneuville A, Muret P and Araujo D 2004 *Phys. Status Solidi* a **201** 2457–61
[61] Lawson S C, Kanda H, Kiyota H, Tsutsumi T and Kawarada H 1995 *J. Appl. Phys.* **77** 1729–34
[62] Teraji T, Katagiri M, Koizumi S, Ito T and Kanda H 2003 *Japan J. Appl. Phys.* **42** L882–4